Characterization and Application of Nanomaterials (2020) Volume 3 Issue 1
doi:10.24294/can.v3i1.716

ORIGINAL RESEARCH ARTICLE

Effect of multiple laser shock processing on nano-scale microstructure of an aluminum alloy

Simge Gencalp Irizalp*, Nursen Saklakoglu

Department of Mechanical Engineering, Celal Bayar University, Manisa Daire 45030, Muradiye, Turkey. E-mail: simge.gencalp@cbu.edu.tr

ABSTRACT

In this study, nano-scale microstructural evolution in 6061-T6 alloy after laser shock processing (LSP) was studied. 6061-T6 alloy plate was subjected to multiple LSP. The LSP treated area was characterized by X-ray diffraction and the microstructure of the samples was analyzed by transmission electron microscopy. Focused Ion Beam (FIB) tools were used to prepare TEM samples in precise areas. It was found that even though aluminum had high stacking fault energy, LSP yielded to formation of ultrafine grains and deformation faults such as dislocation cells, stacking faults. The stacking fault probability (PSF) was obtained in LSP-treated alloy using X-Ray diffraction. Deformation induced stacking faults lead to the peak position shifts, broadening and asymmetry of diffraction. XRD analysis and TEM observations revealed significant densities of stacking faults in LSP-treated 6061-T6 alloy. And mechanical properties of LSP-treated alloy were also determined to understand the hardening behavior with high concentration of structural defects.

Keywords: Laser Shock Processing; Microstructure; Deformation; Stacking Fault

ARTICLE INFO

Article history:
Received March 6 2020
Received in revised form 1 April 2020
Accepted 5 April 2020
Available online 21 April 2020

1. Introduction

Laser shock processing (LSP) is an innovative surface enhancement technique which has been used generally to improve mechanical performance of metallic components. LSP is a method of imparting compressive residual stress under laser shock amplitude loading[1]. Fatigue strength and fatigue life of a metallic material can significantly increase due to the presence of compressive residual stress in the material[2,3]. Also, the generated shock wave can induce severe plastic deformation in the specimen where the shock wave is effective[4,5]. The increase in hardness and yield strength of metallic materials is attributed to high-density dislocation arrays and the formation of twins owing to the shock wave[6-8]. Consequently, high-density dislocations and grain refinement mechanisms are induced in the laser-shocked near-surface microstructure of the metal.

Al-Mg-Si alloys are desirable in aerospace, automotive and shipping industries. Specifically, the 6061-T6 alloy has found widespread application due to a combination of high mechanical strength, low density, and good corrosion resistance[9,10]. It has been reported that compressive residual stress has been observed in 6061-T6 alloy samples under high-strain rate and ultra-high pressure, resulting in considerably improved tribological, fatigue and mechanical properties[5,10-14]. Recently, characterization studies at the nano-scale have become crucial in analyzing the microstructure induced by LSP. The mechanism

for microstructure evolution has a great importance in determining mechanical characteristics, because changes in mechanical characteristics can be understood in regard to microstructure. The sub-structures which create details of the microstructure are influenced by dynamic responses of the material due to shock stress loading[15]. Forming a nano-structure in a polycrystal results in the generation of dislocations, sub-grain structures, dislocation cells and stacking faults (SFs). In severe plastic deformation, the dislocation activity and stacking fault formation mechanism depends on the lattice structure and stacking fault energy probability (P_{SF})[9,16,17]. Chen *et al.*[18] found twin grains with SFs and breaking of large grains into smaller grains in the laser shocked area of 2Cr13Mn9Ni4 austenitic stainless steel. Ye *et al.*[19] found that dislocations were the dominant deformation modes in laser shocked copper foil and they propounded that SFE plays an important role in plastic deformation under conditions of ultrahigh strain rate. He *et al.*[6] noted that high density dislocation lines developed in the original grains caused by the shock wave at high strain rate during LSP.

However, most of the research was concentrated on the residual stress distribution versus depth and fatigue properties in components induced by LSP. The dynamic material response under compressive shock loading has a key role in terms of microstructural features. Microstructural changes at the nano-scale, the mechanism of grain refinement, and the underlying reasons for them have been discussed in previously mentioned reports in very few studies.

The aim of the present study is to investigate nano-scale characterization of LSP-treated materials using transmission electron microscopy (TEM). The grain refinement process under plastic deformation is revealed by considering the SFE of the material. In this regard, deformation mechanisms of LSP-treated materials, such as stacking faults, dislocation configuration and ultrafine grain formation, are investigated. Therefore, in this study, the strengthening mechanism was analyzed quantitatively by X-ray line profile analysis method and supported by TEM observations.

2. Experimental procedures

2.1 Principle and experimental procedure of LSP

The LSP parameters were typically selected to achieve a high power density[21]. Laser power density obtained in our previous experiments[5] was about 16.025 GW/cm^2. The laser pulse was directed through the transparent overlay and interacted with the opaque overlay and a plasma generated on the target material. The opaque overlay protected the sample surface from the thermal effect. The plasma was confined by the transparent overlay which was called "confined ablation"[3,11]. The hydrodynamic expanded plasma in the confined medium between the target material and the confining layer generates a high-pressure pulse. Therefore, a shockwave propagates into the material and the confining medium. When the magnitude of the shock wave exceeds the dynamic yield strength of the metal, plastic deformation occurs in the near surface of the metal[3,4,21]. Plastic deformation modifies the microstructure of specimen in the region affected from shock wave.

2.2 Experimental material and processing parameters

6061-T6 alloy was used in the present work. The thickness of material was 2 mm. The chemical composition of 6061-T6 alloy was shown in **Table 1**. Prior to LSP treatment, the samples were cleaned ultrasonically in ethanol to degrease their surfaces. And then, the specimens were covered with opaque black tape. They were immersed in a water of which the thickness above the target was 2 mm which is called confining medium. The LSP experiments were performed using a pulsed Nd:YAG laser operating at a repetition rate of 10 Hz, a wavelength of 1064 nm and a pulse duration of 6 ns. Laser beam spot diameter on the target was set to 1 mm. The overlapping rate was kept 50% between two laser-beam spots. The LSP procedure was performed in single LSP impact and double LSP impacts. The processing parameters used in LSP were shown in **Table 2**. During LSP, the target was operated in x and y-axis.

Table 1. Composition of 6061-T6 alloy

Si	Fe	Cu	Mn	Mg	Cr	Ni	Zn	Ti
0.62	0.46	0.29	0.09	0.88	0.17	0.01	0.04	0.05

Table 2. The processing parameters used in LSP

Type	Value
Pulse energy (mJ)	750
Spot size (mm)	1
Repetition rate (Hz)	10
Pulse duration (ns)	6
Laser wavelength (nm)	1064
Overlapping rate (%)	50

2.3 Microstructural observations

The microstructure of LSP-treated area of the samples was analyzed by transmission electron microscopy-TEM (FEI Tecnai G2 F30). The right observation within the material depended on significantly TEM specimen preparation technique. Focused Ion Beam (FIB) tools were used to prepare TEM samples in precise areas. The classical techniques for preparing TEM samples are not suitable for the analysis of a specific micrometric area in the specimen[22]. If the classical TEM samples preparation techniques were preferred, the dislocation densities and the dislocation evolution might alter in material microstructure. Therefore, this kind of process was avoided in particular in this work and so FIB was used as sample preparation method.

In TEM specimen preparation process, lift-out is a technique whereby membrane is produced in a thin sample, then cut free using the FIB and removed for stand-alone examination in the TEM. The procedure composes of four steps:

(1) A particular region was located by SEM. During milling which was subsequent step, to protect the investigated feature, platinum, tungsten or other weighty metal layer in order to protect it from deep damaging due to ion irradiation during milling was deposited on the area of interest.

(2) The material surrounding the platinum strip was removed by FIB milling and so a lamella which was performed on thin specimens transparent to electrons was left intact.

(3) A micromanipulator needle was fixed to the sample thanks to a platinum welding and then the lamella was cut free and lifted out of the milled cavity.

(4) The sample was placed in a TEM grid as so contact to the platinum weld, then the connection between lamella and needle was cut[22,23].

The samples of LSP-treated and un-treated were prepared by FIB/SEM (FEI Nova 600i Nano-lab) in attempt to analyze in depth 10 micron and they were made ready for TEM examinations.

2.4 X-Ray diffraction analysis

X-ray diffraction measurements were carried out using the Philips X'Pert Pro equipped with a Cu-Kα radiation source whose wavelength was 1.542Å. X-ray penetration depth is an order of 50μm. The broadening and position shifts of the full-width at half maximum (FWHM) of the α-Al {311} X-ray diffraction peak were considered to obtain the dislocation density, lattice strain, and stacking fault probability. The dislocation density values were obtained from our former study[21]. The lattice strain and the stacking fault probability measurement and calculation were realized on a certain plane in this study, the peaks of the α-Al (311) lattice plane is recommended in X-ray diffraction technique for aluminum alloys because this plane is the intense peak plane from X-ray diffraction data[24]. Lattice strain was calculated by Scherrer equation[25]. This procedure was reported well documented in our previous work[5]. The stacking fault energy γ is inversely proportional to stacking fault probability (P_{SF})[26] and the stacking fault probability was determined by following equation developed by Noskova and Pavlov[27]:

$$P_{SF} = \frac{G a_0^{\,2} d\rho}{24\pi\gamma}$$

Where the stacking fault energy γ consists of the contribution of the stacking fault probability P_{SF}, shear modulus G, lattice constant a_0, lattice space of determined crystal plane$d$, dislocation density ρ.

2.5 Measurements of micro-hardness and tensile properties

The hardness properties of LSP-impacted alloy were investigated by micro-hardness measurement using Vickers-indenter. The tests were

carried out under 50 g load and 10s of the hold time. The hardness measuring was performed on the metal surface. Tensile properties were determined using a Schimadzu testing machine and by a video extensometer. The tensile tests were carried out at a room temperature and a displacement rate 1 mm/min.

3. Results and discussion

Micrographs obtained from TEM examinations, which were performed to investigate the LSP-treated and un-treated 6061-T6 alloy prepared by the FIB technique, are given below.

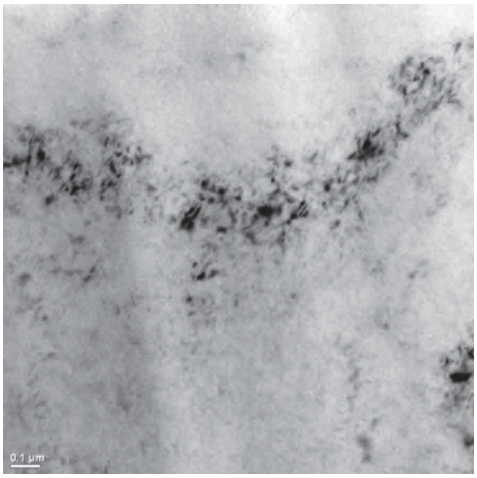

Figure 1. The TEM images of un-treated 6061-T6 alloy: low dense dislocation line**.**

The TEM images of untreated alloy are shown in **Figure 1**. Low-density dislocations are clearly seen. There are low density defects in the microstructure. **Figure 2** shows TEM images which were obtained from single LSP impact. LSP created stacking faults (SF) can be seen in (**Figure 2**). SF is a defect type which affects the mechanical properties of crystalline materials and is commonly seen in materials with low stacking fault energy (SFE)[28]. SFs can be formed during crystal growth, due to acts of partial dislocations during plastic deformation or as a result of separation of total dislocations into two partial dislocations. The dislocation separation distance is related to the magnitude of the SFE. SFs can also be generated by the excess point defects produced in severe plastic deformation or high-strain rate deformation or laser irradiation[28].

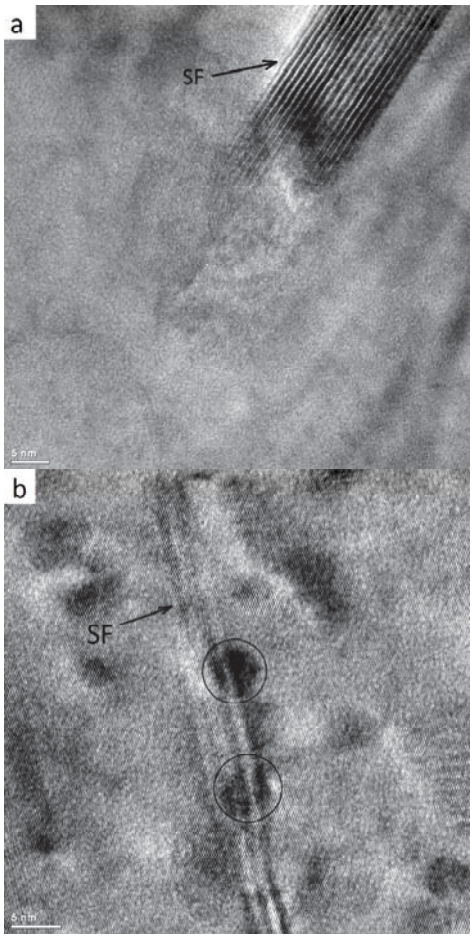

Figure 2. The TEM images of stacking faults in one-LSP impact alloy **(a)** and **(b).**

SFs are local regions of incorrect sequence of crystal planes associated with the presence of partial dislocations. SFs originate from dissociation of dislocations to reduce the elastic energy of the crystal[29]. If the local region formed as a result an incorrect sequence is of a few interatomic distances, it is called a “stacking fault”, and if it is of numerous interatomic distances, it is called “twinning”. While twinning is a dominant deformation mechanism in materials with low-SFE (e.g. copper, brass), it can be rarely formed in materials with high-SFE such as aluminum. Laser shock processing can create a large amount of SFs in 6061-T6 aluminum alloy due to ultra-high plastic strain. In **Figure 2(b)**, multiple dislocation cores interact with the SFs. The indicated regions in **Figure 2(b)**, which are shaped like dark circles, are trapped dislocations. The trapped dislocations indicated with circles intercept the SF plane.

When **Figure 3** was observed, it was seen that the dislocations were organized and these well-organized dislocations created the dislocation

cell walls. Ren *et al.*[30] observed band-like dislocation walls in TEM observations which performed in LSP GH2036 and they reported that the dislocation walls coincident with slip planes. When **Figure 3(a)** and **3(b)** were examined, the dislocation walls having tangled dislocation boundaries attracted the attention in the single LSP impacted 6061-T6 alloy and also looked band-like. The dislocation cell formation notably reduces the stored energy in deformed crystallites[31]. For this reason, the high energy induced by the LSP into the material tends to create dislocation cells.

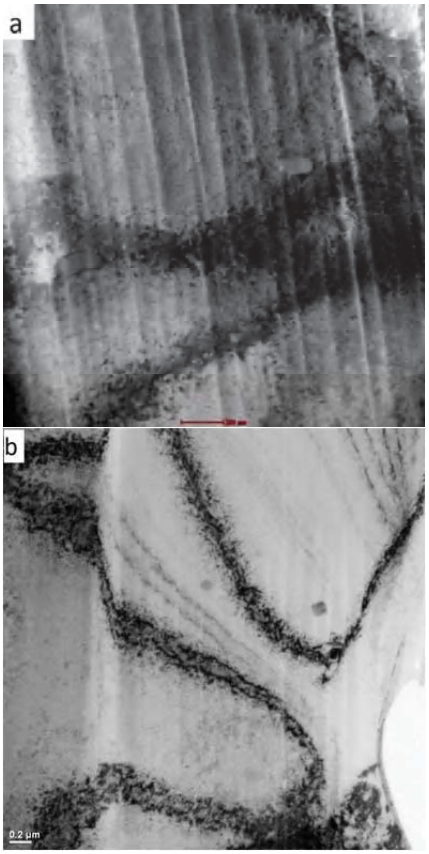

Figure 3. The TEM images of the well-organized dislocation cell walls and subgrain structures**.**

It was observed that dislocation tangled zones occurred and heavily deformed subgrain structures derived from dislocation cell structures induced in laser shock processing. Shin *et al.*[32] stated that cell boundary can originate from severely tangled dislocations and therefore subgrains induced. It was seen that the subgrains of which size is about 300-800 nm in **Figure 3(a)**. And also, when the cell structure was observed, it was realized that the high density dislocations existed at the boundary but the low density dislocations observed inside. The severe plastic deformation induced by LSP caused the dislocation piping and induced heavily tangled dislocation lines and consequently, dense dislocation walls occurred. The white lines which are seen in **Figure 3** are certain effect and originated from FIB preparation process.

Lu *et al.*[33], Wang *et al.*[34] and Liu *et al.*[35] argued that the subgrain boundaries developed by dislocation transformation. It is known that the stacking faults formed among partial dislocations in FCC metals[36]. Sun *et al.*[37] stated that there were two factors governing the grain refinement: stacking fault energy and slip system numbers. Lu *et al.*[38] remarked that the dislocation cell formation in the metals which have medium SFE results in grain refinement. In high SFE metals, dislocation walls and tangles formation leads to the refinement mechanism but SF formation is difficult. In consequence, plastic deformation behavior of the materials depends strongly on the SFE[38]. During severe plastic deformation, the point defections and SFs in the crystal interact with each other and new atoms move on SF region. Therefore, new atoms located and grouped in the SF and so stacking fault energy is decreased, and partial dislocations were opened and resulted in stacking fault ribbon widening[36].

The deformation microstructure of face-centered cubic materials is complex. Many grains in face-centered cubic materials have sharp grain boundaries and non-uniform sized grains[35]. It was also seen that organized dislocations and dislocation cells formed in **Figure 4**. Dislocation cells corresponded to sub-grain formation in the TEM investigations. Growth of cellular microstructure is formed by separation from organized dislocations[39]. The term “cell” usually refers to small volumes formed by diffuse dislocation boundaries, and also the term“subgrain” refers to bounding more organized dislocations. Dislocation cells which organized after deformation correspond to the “subgrain”. Comparing with untreated alloy, it is obvious that the dislocation arrangements in the networks become more complex and tangled. High-density dislocation lines, a dislocation network and a dislocation wall which

corresponds to a sub-grain boundary can be clearly seen in one-impact LSP. Stacking faults can be formed by the homogenous mechanism enhancing the possibilities of the material to respond to dynamic loading. Severe plastic deformation formed obvious stacking faults while aluminum has high SFE.

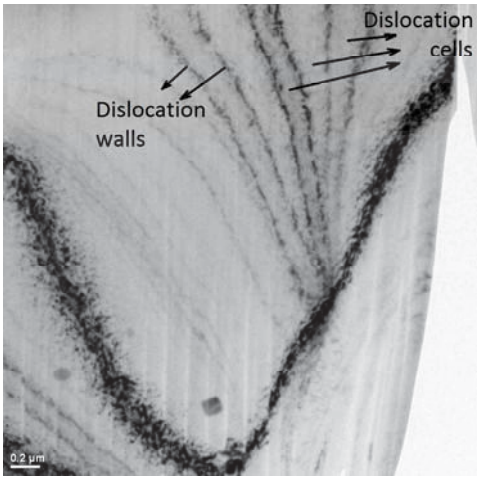

Figure 4. The TEM images of the organized dislocation and dislocation cells in single LSP impact alloy**.**

The TEM images of double-LSP impact alloy were given in **Figure 5**. Nano grain with size of 40-50 nm which contains trapped dislocations (white arrows) is seen in **Figure 5(a)** and **Figure 5(b)** shows both ultrafine grains with size of 200-300 nm and nano-grain having size of about 50 nm. This TEM image showed that ultrafine grains can be deformed by dislocation motion. The ultra-fine grains and nano-grains have darker contrast in comparison to micro-sized grains. Because the ultrafine size leads to randomly oriented grains, therefore, allows the variations in dynamical diffracting conditions[31,40]. The ultrafine grains contain high internal stress and this situation gets elastic distortions in crystal lattice[31]. Higher density dislocation regions especially induced by severe plastic deformation are in accordance with higher mis-orientations. The subgrain boundaries disturb the deformation coordination and higher density dislocations accumulated and rearranged, thus, lower angle subgrain boundaries induced by plastic strain increasing. Finally, finer grains are formed[41].

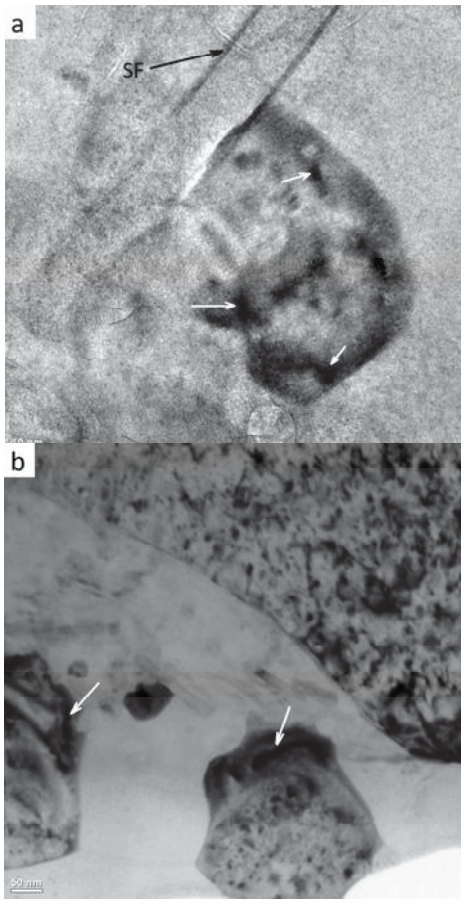

Figure 5. TEM micrograph of trapped dislocations in a nano-grain: **(a)** nano-grains and ultrafine grains, **(b)** in double LSP impact alloy**.**

After double LSP impact, rearrangement of dislocations occurs and leads to newly ultrafine grains. Local distortions in terms of trapped dislocations are clearly visible in the TEM micrograph. The main cause for the locally distributed/trapped dislocations is associated with the energy stored during plastic deformation at nano-scale in the lattice structure[42]. Therefore, the short duration of plastic deformation under the localized load is responsible for the dislocation trapping in the nano-scale structure. The development of the dislocations during LSP process was clearly seen in **Figure 6**. Low-density dislocations in high magnification attract the attention for un-treated alloy in **Figure 6(a)**. Tangled and dense dislocation arrangements were seen in the laser shocked region (**Figure 6(b)** and **(c)**).

Comparing the microstructures, the one-LSP impact treated specimen presents some dislocations which have discrete structure and are small in length and the double LSP impact treated specimen presents the distinctively different char-

acteristics which are longer and more complex in shape and it has dislocation nodes.

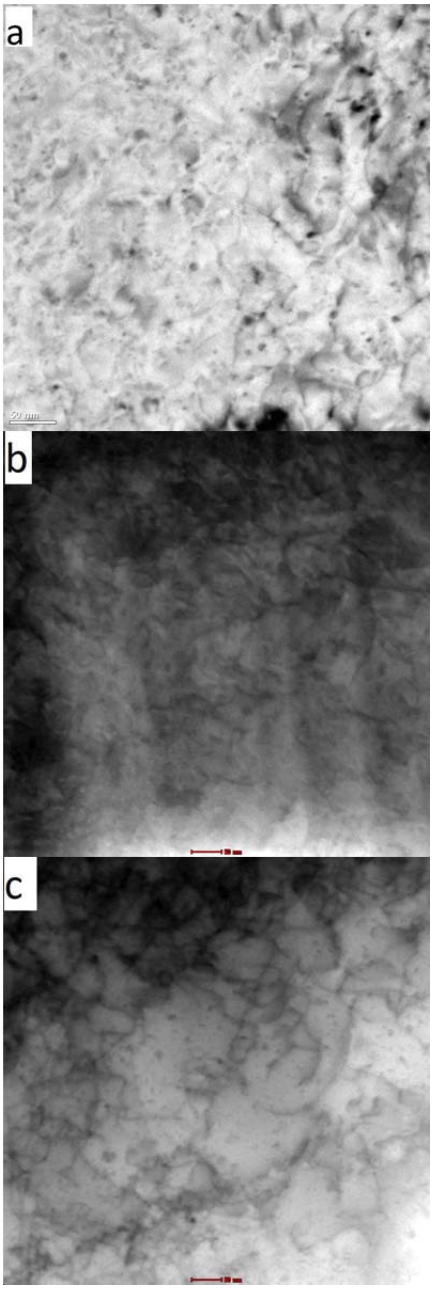

Figure 6. TEM image of dislocations : **(a)** un-treated alloy, **(b)** single-LSP impacted alloy, **(c)** double LSP-impacted alloy**.**

The tangled dislocations were also observed to dissociate into partial dislocations. Chen *et al.*[43] found that the deformation generated adjacent local areas with different orientations when the metal was exposed to plastic deformation. In consequence of laser shock processing, crystallites which had low-angle orientation boundaries were generated in the near-surface regions. Thus, nano-grains with different orientation were produced inns-pulsed laser experiments. Formation of nano-crystalline structures in aluminum alloy after laser shock processing broadly was investigated by X-ray line profile analysis in our previous work[21].

Figure 7 shows the diffraction peak profiles of (311) for untreated, single LSP impacted and double LSP impacted alloy and this diffraction profiles were received from our previous work[21]. Peak broadening and shifts are clear as a result of laser shock processing. Line broadening analysis of XRD peaks explores the crystallite size which for samples with lattice faults[21]. Moreover, the peak broadening analysis was also used to determine the stacking fault probability (P_{SF})[44-46]. The peak shift and broadening were affected from randomly oriented crystallites with small faulting probabilities[44]. The Bragg's law and equation (1) were used for calculations and the values of d-spacing, stacking fault probability and lattice strain for all the samples were listed in **Table 3**. The values of dislocation density in **Table 3** received from our previous work[21]. The deformed material during laser shock processing, and the non-uniform strain happened in the crystal lattice led to a broadening in FWHM of X-ray diffraction peak. The lattice strain is defined as the increment of inter-planar spacing and as a function of the exposed strain[44]. Moreover, lattice strain can be expressed as micro-strain of the lattice deformation[47]. According to **Figure 7**, lattice strains considerably affected the diffraction peak profiles as a broadening in FWHM after LSP. As it is known, high strain rate deformation causes lattice distortion and work hardening. Lattice distortion brings the dislocations and new grain boundaries[48].

In low SFE materials, stacking faults and twin formation play an important role in the formation of nanostructures and ultrafine grains[49-52]. Coarse grained FCC metals with high stacking fault energy such as aluminum is anticipated to deform by dislocation slip. However, when the material was deformed in high strain rate deformation condition, the stacking fault and twin formation conditions have improved. At the same time, the high strain rate deformation condition contributed to nano-crystalline formation. Shock deformation has been found to produce twins and

stacking faults in medium-high stacking fault energy alloys[53].

Table 3. X-ray line profile analysis results of 6061-T6 alloy

	2θ of (311) plane[21]	Dislocation density, $\rho_{dis}\rho_{dis}$ (10^{14} lines/m^2)[21]	Lattice strain,ε	d-spacing (nm)	Stacking fault probability, P_{SF}
Un-treated	78.166	7.367	0.089	0.78774	0.02183
Single LSP impact	78.100	18.437	0.141	0.78793	5.4668
Double LSP impact	78.034	19.092	0.143	0.78812	5.6624

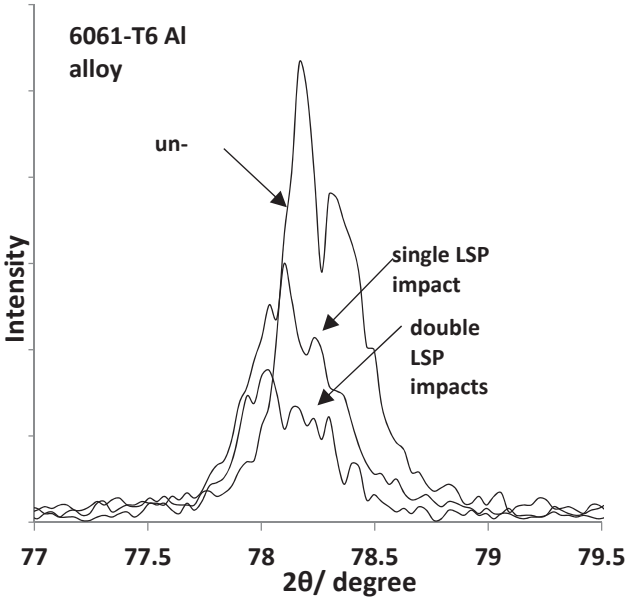

Figure 7. X-ray diffraction patterns (311) of 6061-T6 alloy subjected to various LSP impacts[21].

Atultra-high strain rate, the energy required for the motion of a perfect dislocation is higher than that required for the motion of two partial dislocations formed by the decomposition of a perfect dislocation. As it is known, the formation of the stacking faults is inversely depended on the stacking fault energy. Therefore, low SFE and high stacking error probability lead to the formation of a large number of stacking errors[18]. Wert *et al.*[54] stated that the particle size decreased with decreasing SFE, while the stacking fault probability increased.

Figure 8 shows the variation in the stacking fault probability (P_{SF}), lattice strain (ε), and dislocation density (ρ_{dis}) as a function of process parameters. As shown in **Figure 8(a)**, the dislocation density was 7.367x10^{14} m^{-2} for the untreated alloy. The dislocation density value strongly increased via laser shock processing. It was reached the ρ_{dis} value of 19.092 x10^{14} m^{-2} with double shot LSP impact. **Figure 8(b)** shows the evolution of the lattice strain (ε) increased after LSP treatment. The increase in ε indicates that the severe lattice distortion introduced during LSP yielded tore-arrangement of dislocation. **Figure 8(c)** shows the evolution of the stacking fault probability (P_{SF}) increased after LSP treatment.

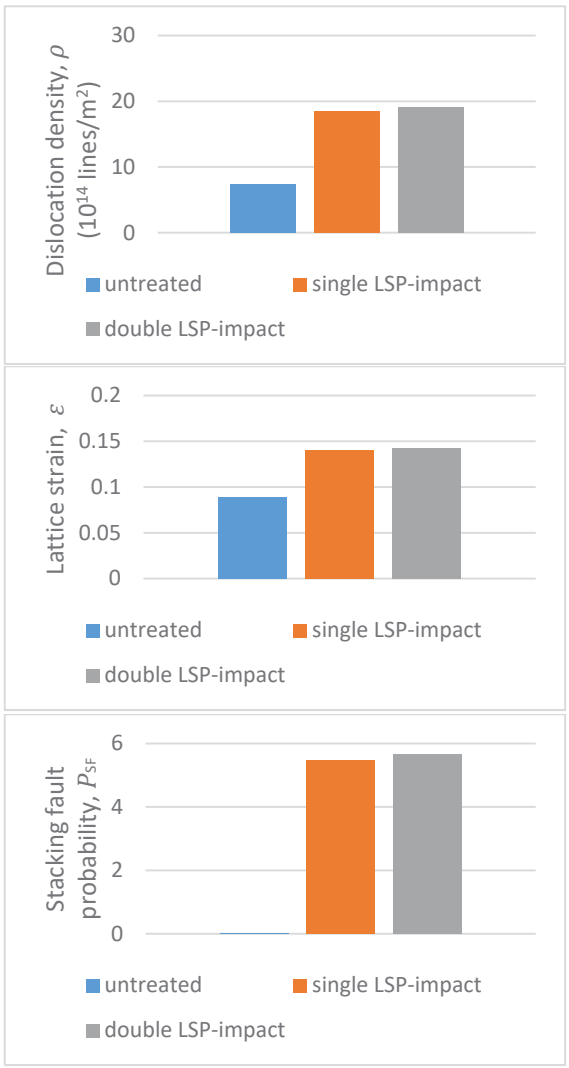

Figure 8. Plot showing the variation of **(a)** dislocation density, **(b)** latticestrain, and **(c)** stacking fault probability with process parameter for 6061-T6 alloy**.**

The stacking fault probability was also obtained from the peak asymmetry of (311) Bragg's peak. The stacking fault probability in 6061-T6 alloy increased sharply with LSP treatment. Thus, the increase in stacking fault probability in 6061-T6 alloy will decreased the SFE after high strain rate deformation[55-56].

There are five main strengthening mechanism in the metallic materials: solid-solution hardening, precipitation hardening, transformation hardening, dislocation hardening and grain refinement[57-58]. The solid-solution hardening and precipitation hardening did not significantly affect the strength of the exposed specimen. The dislocation hardening and grain refinement brings a significant increase in the materials strength. When the stress applied to the material exceeds the yield strength, perfect dislocations both move and multiply. In alloys with low stacking fault energy, a perfect dislocation dissociates into two dislocations and two extended dislocations form. When two extended dislocations on the conjugate slip planes intersect each other, extended jogs and Cottrell ± Lomer locks are formed. They prevent the movement of dislocations and so an increase in the strain hardening occurs. The lower the SFE is, the higher the stacking fault probability is, and the wider the stacking fault ribbons is, resulting in more difficult cross slip, increased strain hardening and prolonged linear hardening stage[59].

Table 4. Mechanical properties of LSP impacted 6061-T6 alloy

Parameters	Surface hardness ($HV_{0.05}$)	UTS (MPa)	YS (MPa)
Untreated	97	214	177
Single LSP-impact	113	316	280
Double LSP-impact	121	312	286

Examinations of the mechanical properties have indicated work hardening behavior of LSP impacted materials. When **Table 4** examined, mechanical properties have been improved effectively by LSP. After single LSP-impact, its surface hardness improved from 97 $HV_{0.05}$ to 113 $HV_{0.05}$ and after double LSP impact, improved to 121 $HV_{0.05}$. And also, after LSP treatment, UTS approximately increased 45%, and YS increased 60%. The mechanical properties of LSP after impact are not only due to the increase of stacking fault probability, but also due to the significant increase of dislocation density and lattice strain. High density dislocation arrangement and also new ultrafine grain structure reveal the strengthening mechanism. But in this study, it is not enough to explain the behavior of strengthening with only grain refinement and high density dislocation. In the high strain rate process, LSP treatment increases PSF value (**Figure 8(c)**). The dramatic increase in stacking fault probability has triggered the formation of stacking faults. High P_{SF} is associated with a decrease in stacking fault energy. As it is known, partial dislocations were opened with SFE decreasing and the SFE formation was launched by the interaction between partial dislocations and point defections. The SFE of FCC metal was decreased, and the dislocation accumulation and stacking accumulation were decreased, and the work hardening behavior was improved[38]. The dislocation accumulation, accumulated SFs and ultrafine grain structure provided the extra strengthening. These inferences are in good agreement with TEM observations. XRD line analysis is an effective method for the determination of SF, grain size, lattice strain and dislocation density[5,57,60]. The SF strengthening, nanostructure and ultrafine grained microstructure were obtained after severe plastic deformation (SPD), equal channel angular pressing (ECAP), and high-pressure torsion (HPT)[61-64]. In this study, sheet metal samples were exposed to high strain rate by LSP method which is applied to the industry and a significant strengthening behavior was induced by microstructural development of the material.

Figure 9 shows the stacking faults in atomic resolution. Liao *et al.* and Lee *et al.*[65-66] reported the typical stacking faults in atomic level image. The SF width in **Figure 9(a)** was about 0.4 nm and in **Figure 9(b)** was about 0.7 nm. It is seen that the double LSP impact is responsible for the wide SF. The lowering SF energy led to a wider stacking fault and higher stacking fault probability. SFs interact with point defections in the crystal. During the mechanical reaction in the material through several plastic deformations, new atoms move towards SF region and so elastic-energy of the crystal reduces. This formation occurring between the partial dislocations causes a reciprocal push of the partial dislocations, which lowers the SFE, so that a widening of the SF band can be observed[36]. Partial dislocations restricted by a stacking fault ribbon[66].

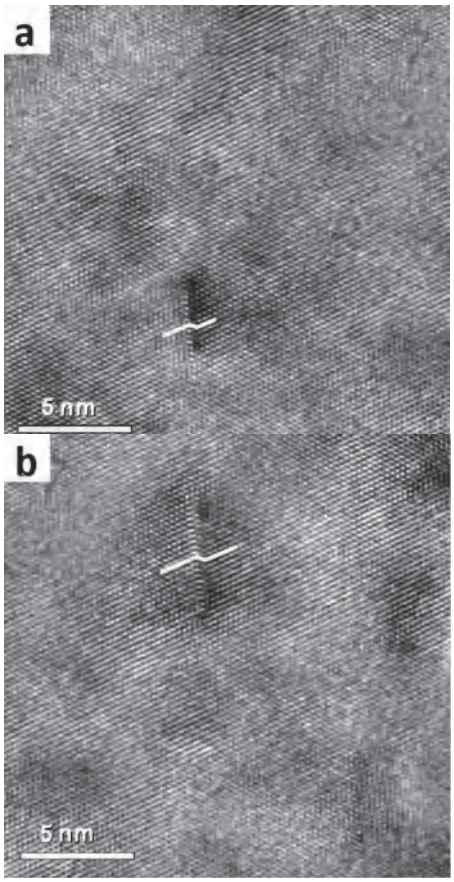

Figure 9. Atomic level image of a typical stacking faults after **(a)** single LSP impact and **(b)** double LSP impact**.**

In this study, stacking fault bands can be observed during laser shock treatment with high-strain rates, even if the material was a high SFE metal. Ye *et al.*[19] reported that dislocation slip was the dominant deformation mode at small-strain conditions. However, under shock conditions, stacking faults and twins were formed besides dislocation slip. In terms of microstructural observations, dislocation cells, and stacking faults subdivide the initial coarse grain into randomly ultra-refined grains. High-strain rate and a short duration laser pulse play an important role in the formation of refined grains during micro plastic deformation by LSP.

4. Conclusions

The aims of the present work were to investigate the formation of dislocations, dislocation cell structures, lattice orientations and sub-structures at the nano-scale under shock loading. TEM investigations demonstrated the formation of stacking faults, dislocation arrangements and ultrafine grains. Multiple LSP impacts at high-strain rate created more dislocations, which could generate stacking faults, nano-grain and ultrafine grain structures. The main results showed that the stacking fault probability significantly increased from 0.02183 to 5.6624 and dislocation density increased from 7.367 to 19.092 after LSP treatment. Microstructural parameters were also in good agreement with the results of X-ray line profile analysis. The short duration and high pressure effect of plastic deformation under the localized load lead to the trapping of dislocations in nano-scaled structures. The LSP results presented highly tangled and dense dislocations and dislocation cell-structures. It clearly showed the hardness increment in LSP treatment material. This increment resulted from grain refinement, dense dislocation structure and stacking faults. Experimental observations and evidence of the grain refinement mechanism demonstrated that a high-SFE metal which was deformed at high-strain rates could form ultrafine grains, and stacking faults.

Acknowledgments

The authors would like to thank Celal Bayar University (Project Code: 2012-009) for providing financial support. They would also like to thank for the financial support given to Laser Technologies Research and Application Center (LATARUM).

References

1. Ren X, Zhang Y, Zhang T, *et al.* Comparison of the simulation and experimental fatigue crack behaviors in the nanoseconds laser shocked aluminum alloy. Materials & Design 2011; 32(3): 1138–1143.
2. Yang C, Hodgson PD, Liu Q, *et al.* Geometrical effects on residual stresses in 7050-T7451 aluminum alloy rods subject to laser shock peening. Journal of Materials Processing Tech 2008; 201(1-3): 303–309.
3. Ye L, Ding K. Laser shock peening: Performance and process simulations. Cambridge: Woodhead Publishing; 2006. p. 172.
4. Lu J, Luo K, Zhang Y, *et al.* Grain refinement mechanism of multiple laser shock processing impacts on ANSI 304 stainless steel. Acta Materialia 2010; 58(16): 5354–5362.
5. Irizalp SG, Saklakoglu N, Yilbas BS. Characterization of microplastic deformation produced in 6061-T6 by using laser shock processing. Interna-

tional Journal of Advanced Manufacturing Technology 2014; 71(1-4): 109–115.
6. He T, Xiong Y, Guo Z, *et al.* Microstructure and hardness of laser shocked ultra-fine-grained aluminum. Journal of Materials Science & Technology 2011; 27(9): 793–796.
7. Chu JP, Rigsbee JM, Bana G, *et al.* Laser-shock processing effects on surface microstructure and mechanical properties of low carbon steel. Materials Science & Engineering A 1999; 260(1-2): 260–268.
8. Li Y, Zhou L, He W, *et al.* The strengthening mechanism of a nickel-based alloy after laser shock processing at high temperatures. Science & Technology of Advanced Materials 2013; 14(5): 1–9.
9. Ren X, Ruan L, Yuan S, *et al.* Dislocation polymorphism transformation of 6061-T651 aluminum alloy processed by laser shock processing: Effect of tempering at the elevated temperatures. Materials Science & Engineering 2013; 578: 96–102.
10. Sathyajith S, Kalainathan S, Swaroop S. Laser peening without coating on aluminum alloy Al-6061-T6 using low energy Nd: YAG laser. Optics & Laser Technology 2013; 45: 389–394.
11. Gencalp Irizalp S, Saklakoglu N, Akman E, *et al.* Pulsed Nd: YAG laser shock processing effects on mechanical properties of 6061-T6 alloy. Optics & Laser Technology 2014; 56: 273–277.
12. Rubio-Gonzalez C, Gomez-Rosas G, Ocana JL, *et al.* Effect of an absorbent overlay on the residual stress field induced by laser shock processing on aluminum samples. Applied Surface Science 2006; 252(18): 6201–6205.
13. Rubio-Gonzalez C, Ocana JL, Gomez-Rosas G, *et al.* Effect of laser shock processing on fatigue crack growth and fracture toughness of 6061-T6 aluminum alloy. Materials Science and Engineering: A 2004; 386(1-2): 291–295.
14. Sanchez-Santana U, Rubio-Gonzalez C, Gomez-Ro sas G, *et al.* Wear and friction of 6061-T6 aluminum alloy treated by laser shock processing. Wear 2006; 260(7-8): 847–854.
15. Kalantar DH, Belak J, Bringa E, *et al.* High-pressure, high-strain-rate lattice response of shocked materials. Physics of Plasmas 2003; 10(5): 1569–1576.
16. Cao XJ, Pyoun YS, Murakami R. Fatigue properties of a S45C steel subjected to ultrasonic nanocrystal surface modification. Applied Surface Science 2010; 256(21): 6297–6303.
17. Zehetbauer M, Valiev RZ. Nanomaterials by severe plastic deformation. Weinheim, Berlin: Wiley-VCH; 2004. p. 1–850.
18. Chen K, Zheng C, Yuan Z, *et al.* Deformation microstructures of austenitic stainless steel 2Cr13-Mn9Ni4 under ultrafast strain rate by laser shock processing. Materials Science and Engineering A: Structural Materials: Properties, Microstructure and Processing 2013; 587: 244–249.
19. Ye Y, Feng Y, Lian Z, *et al.* Plastic deformation mechanism of polycrystalline copper foil shocked with femtosecond laser. Applied Surface Science 2014; 309: 240–249.
20. Yilbas BS, Arif AFM, Shuja CZ, *et al.* Investigation into laser shock processing. Journal of Materials Engineering and Performance 2004; 13: 47–54.
21. Saklakoglu N, Gencalp Irizalp S, Akman E, *et al.* Near surface modification of aluminum alloy induced by laser shock processing. Optics & Laser Technology 2014; 64: 235–241.
22. Jublot M, Texier M. Sample preparation by focused ion beam micromachining for transmission electron microscopy imaging in front-view. Micron 2014; 56: 63–67.
23. Grassian VH (editor). Nanoscience and Nanotechnology. Bridgewater, New Jersey: John Wiley & Sons, Inc.; 2008. p. 461.
24. Committe AIH. Metals handbook volume 10 — Materials characterization. Fifth Printing. Novelty, Ohio: ASM Int; 1998. p. 1310.
25. Fultz B, Howe JM. Diffraction lineshapes. In: Transmission electron microscopy and diffractometry of materials. 4th ed. Berlin Heidelberg: Springer; 2013. p. 429–462.
26. Zhou W, Jiang B, Liu Y, *et al.* Stacking fault probability and stcaking fault energy in CoNi alloys. Transactions of Nonferrous Metals Society of China 2001; 11(4): 555–558.
27. Noskova NI, Pavlov VA. Stacking faults in nickel solid solutions. Physics Metal and Metallography 1962; 14: 86.
28. Li B, Yan P, Sui M, *et al.* Transmission electron microscopy study of stacking faults and their interaction with pyramidal dislocations in deformed Mg. Acta Materialia 2010; 58(1): 173–179.
29. Hull D, Bacon DJ. Introduction to dislocations. 3rd ed. Oxford, United Kingdom: Pergamon Press. 1984. p. 80.
30. Ren X, Zhou W, Ren Y, *et al.* Dislocation evolution and properties enhancement of GH2036 by laser shock processing: Dislocation dynamics simulation and experiment. Materials Science & Engineering: A 2016; 654: 184–192.
31. Xu Z, Liu M, Jia Z, *et al.* Effect of cryorolling on microstructure and mechanical properties of a peak-aged AA6082 extrusion. Journal of Alloys and Compounds 2017; 695: 827–840.
32. Shin DH, Park JJ, Kim YS, *et al.* Constrained groove pressing and its application to grain refinement of aluminum. Materials Science & Engineering: A 2002; 328(1-2): 98–103.
33. Lu J, Luo K, Zhang Y, *et al.* Grain refinement of LY2 aluminum alloy induced by ultra-high plastic strain during multiple laser shock processing impacts. Acta Materialia 2010; 58(11): 3984–3994.
34. Wang J, Zhang Y, Chen J, *et al.* Effect of laser sho- ck peening on the high-temperature fatigue performance of 7075 aluminum alloy. Materials Science & Engineering: A 2017; 704: 459–468.
35. Liu M, Roven HJ, Yu Y, *et al.* Deformation struc-

tures in 6082 aluminium alloy after severe plastic deformation by equal-channel angular pressing. Materials Science & Engineering: A 2008; 483-484: 59–63.
36. Gencalp Irizalp S, Saklakoglu N. High strength and high ductility behavior of 6061-T6 alloy after laser shock processing. Optics & Lasers in Engineering 2016; 77: 183–190.
37. Sun H, Shi Y, Zhang M, *et al.* Plastic strain-induced grain refinement in the nanometer scale in a Mg alloy. Acta Materialia 2007; 55(3): 975–982.
38. Lu K, Lu J. Nanostructured surface layer on metallic materials induced by surface mechanical attrition treatment. Materials Science & Engineering: A 2004; 375-377: 38–45.
39. Hurley PJ, Humphreys FJ. Modelling the recrystallization of single-phase aluminium. Acta Mater 2003; 51(13): 3779–3793.
40. Zhang X, Hu T, Rufner JF, *et al.* Metal/ceramic interface structures and segregation behavior in aluminum-based composites. Microscopy and Microanalysis 2015; 21(S3): 1053–1054.
41. Zhang Y, Jiang S. The mechanism of inhomogeneous grain refinement in a NiTiFe shape memory alloy subjected to single-pass equal-channel angular extrusion. Metals 2017; 7(10): 400.
42. Youssef KM, Scattergood RO, Murty KL, *et al.* Ultrahigh strength and high ductility of bulk nanocrystalline copper. Applied Physics Letters 2005; 87(9): 1–3.
43. Chen H, Yao YL, Kysar JW. Spatially resolved characterization of residual stress induced by micro scale laser shock peening. Journal of Manufacturing Science and Engineering 2004; 126 (2): 226–236.
44. Jeong JS, Woo W, Oh KH, *et al.* In situ neutron diffraction study of the microstructure and tensile deformation behavior in Al-added high manganese austenitic steels. Acta Materialia 2012; 60(5): 2290–2299.
45. Tomota Y, Tokuda H, Adachi Y, *et al.* Tensile behavior of TRIP-aided multi-phase steels studied by in situ neutron diffraction. Acta Materialia 2004; 52(20): 5737–5745.
46. Jeong JS, Koo YM, Jeong IK, *et al.* Micro-structural study of high-Mn TWIP steels using diffraction profile analysis. Materials Science & Engineering: A 2011; 530: 128–134.
47. Rafaja D, Siıma M, Klemm V, *et al.* X-ray diffraction on nanocrystalline $Ti_{1-x}Al_xN$ thin films. Journal of Alloys and Compounds 2004; 378(1-2): 107–111.
48. Nie X, He W, Zhou L, *et al.* Experiment investigation of laser shock peening on TC6 titanium alloy to improve high cycle fatigue performance. Materials Science & Engineering: A 2014; 594: 161–167.
49. Huang C, Hu W, Yang G, *et al.* The effect of stacking fault energy on equilibrium grain size and tensile properties of nanostructured copper and copper–aluminum alloys processed by equal channel angular pressing. Materials Science & Engineering: A 2012; 556: 638–647.
50. Das J. Evolution of nanostructure in α-brass upon cryorolling. Materials Science and Engineering: A 2011; 530: 675–679.
51. Roy B, Kumar NK, Nambissan PMG, *et al.* Evolution and interaction of twins, dislocations and stacking faults in rolled α-brass during nanostructuring at sub-zero temperature. AIP Advances 2014; 4(60): 1–8.
52. Kumar NK, Roy B, Das J. Effect of twin spacing, dislocation density and crystallite size on the strength of nanostructured α-brass. Journal of Alloys and Compounds 2015; 618: 139–145.
53. Zhu Y, Liao X, Wu X. Deformation twinning in nanocrystalline materials. Progress in Materials Science 2011; 57(1): 1–62.
54. Wert JJ, Singerman SA, Caldwell SG, *et al.* An X-ray diffraction study of the effect of stacking fault energy on the wear behavior of Cu-Al alloys. Wear 1983; 92(2): 213–229.
55. Talonen J, Hanninen H. Formation of shear bands and strain-induced martensite during plastic deformation of metastable austenitic stainless steels. Acta Materialia 2007; 55(18): 6108–6118.
56. Gong Y, Wen C, Wu X, *et al.* The influence of strain rate, deformation temperature and stacking fault energy on the mechanical properties of Cu alloys. Materials Science & Engineering: A 2013; 583: 199–204.
57. Yamanaka K, Mori M, Sato S, *et al.* Stacking-fault strengthening of biomedical Co–Cr–Mo alloy via multipass thermomechanical processing. Scientific Reports 2017; 7(1): 1–13.
58. Lu K, Lu L, Suresh S. Strengthening materials by engineering coherent internal boundaries at the nanoscale. Science 2009; 324(5925): 349–352.
59. Jiang B, Qi X, Yang S, *et al.* Effect of stacking-fault probability on martensitic transformation and shape memory effect in Fe-Mn-Si based alloys. Acta Materialia 1998; 46(2): 501–510.
60. Mahato B, Shee SK, Sahu T, *et al.* An effective stac- king fault energy viewpoint on the formation of extended defects and their contribution to strain hardening in a Fe–Mn–Si–Al twinning-induced plasticity steel. Acta Materialia 2015; 86: 69–79.
61. Valiev RZ, Islamgaliev RK, Alexandrov IV. Bulk nanostructured materials from severe plastic deformation. Progress in Materials Science 2000; 45(2): 103–189.
62. Liao X, Zhao Y, Zhu Y, *et al.* Grain-size effect on the deformation mechanisms of nanostructured copper processed by high-pressure torsion. Journal of Applied Physics 2004; 96(1): 636–640.
63. Azushima A, Kopp R, Korhonen A, *et al.* Severe plastic deformation (SPD) processes for metals. CIRP Annals 2008; 57(2): 716–735.
64. Lugo N, Llorca N, Cabrera JM, *et al.* Micro structures and mechanical properties of pure copper deformed severely by equal-channel angular pressing and high pressure torsion. Materials Scien-

ce & Engineering A 2008; 477(1-2): 366–371.
65. Liao X, Zhou F, Lavernia EJ, *et al.* Deformation mechanism in nanocrystalline Al: Partial dislocation slip. Applied Physics Letters 2003; 83(4): 632–634.
66. Lee ML, Simmonds PJ. Tensile strained III-V self-assembled nanostructures on a (110) surface. Nano-epitaxy: Homo- and Heterogeneous Synthesis, Characterization, and Device Integration of Nano-materials 2010; 7768: 5.